

## Hydrogen sorption and electrochemical properties of Ti-Fe based alloys synthesized by mechanical alloying

B. Abrashev<sup>1\*</sup>, T. Spassov<sup>2</sup>, M. Pandev<sup>1</sup>, S. Vassilev<sup>1</sup>, A. Popov<sup>1</sup>

<sup>1</sup>Acad. Evgeni Budevski Institute of Electrochemistry and Energy Systems, Bulgarian Academy of Sciences, 10, Acad. G. Bonchev St., Sofia 1113, Bulgaria

<sup>2</sup>Faculty of Chemistry and Pharmacy, University of Sofia "St. Kl. Ohridski", 1 James Bourchier str. 1164 Sofia, Bulgaria

Received March 6, 2017      Revised April 4, 2017

The composite nanocrystalline-amorphous TiFe alloys were obtained mechano-chemically by high-energy ball milling in a planetary type mill. The duration of milling was varied with the aim to produce alloys with defined microstructure. The average size of the powders was reduced from 50 μm to <1 μm after 30-40 hours of grinding. The end product of milling consists mainly of nanocrystalline fcc Ti-Fe with CsCl-type structure. Presence of nanocrystalline Fe was also detected. The synthesised composite material showed relatively high thermal stability. The electrochemical hydrogen charge-discharge behaviour of materials with different microstructure was investigated. It was found out that small microstructural changes result in significant discharge capacity and cycling stability differences. The material milled for 40 hours revealed discharge capacity comparable to that of alloy milled for 30 hours, but its stability was greatly improved.

**Key words:** TiFe alloys, discharge capacity, hydrogen storage.

### INTRODUCTION

Hydrogen has attracted a great deal of consideration in the recent years as a feasibly ideal energy carrier. Its application for mobility and portable electronics is to a large extent limited by the difficulty of achieving a capable storage method. AB, AB<sub>2</sub>, AB<sub>5</sub> and A<sub>2</sub>B-type hydrogen storage compounds and related substituted multi-component alloys have been extensively studied in the last 3-4 decades. As a result, the electrodes prepared from AB<sub>5</sub> (LaNi<sub>5</sub>)- and AB<sub>2</sub> (ZrV<sub>2</sub>)-type alloys have already been commercialised in the rechargeable nickel-metal hydride (Ni/MH) batteries. In general, the titanium-based alloys are among the most promising materials for hydrogen storage. The main representative of AB alloys is an intermetallic compound with TiFe composition, which crystallizes in the cubic CsCl-type structure and is lighter and cheaper than the LaNi<sub>5</sub> alloy [1-6]. AB-type alloys require a preliminary activation treatment, being a disadvantage of the TiFe-based alloys. The activation procedure involves heating of TiFe to a high temperature (about 450°C) in vacuum and annealing in H<sub>2</sub> atmosphere at certain pressure (about 7 bar) [7-14]. The AB-type of alloys can be synthesized by using different

laboratory methods. The most commonly used ones are: arc melting and mechano-chemical synthesis. The method of mechanical alloying (MA) by using high-energy ball milling in a planetary mill verified itself to be an effective technique for both synthesis and modification of the intermetallic hydrogen storage compounds [15]. The application of mechanical alloying under inert atmosphere with the use of catalytic elements, as for instance Pd, rapidly improved the activation process and the hydriding kinetics of TiFe. By ball milling under Ar (20-30 hours) of TiFe with small amounts of Ni, easy hydrogen absorption without activation is achieved. The radical improvement of the kinetics is caused by the formation of a fine powder of TiFe covered by nanocrystalline Ni particles, acting as catalytic centres for the decomposition of H<sub>2</sub> molecules [4]. A lot of effort has been devoted to the studying of the kinetics of metal hydrides [16-25]. Currently, the nickel-metal hydride (Ni/MH) battery systems are perceived as one of the most promising for mobility applications. The advantages of the system relate to high energy density, high rate capacity, good overcharge and overdischarge capability, no electrolyte consumption during charge/discharge cycling and lack of poisonous heavy metals [26-32]. Generally speaking, the rechargeable nickel-metal hydride battery has a similar design to that of nickel-cadmium system (Ni/Cd) but with the principal difference that the Ni/MH uses hydrogen absorbed

---

To whom all correspondence should be sent:  
E-mail: babrashev@iees.bas.bg

in a metal alloy for the active negative material in place of cadmium in the Ni/Cd battery design. The active material of the positive electrode of the Ni/MH battery is nickel oxy-hydroxide (NiOOH) in the charged state. The negative active material in the charged state is hydrogen: in the form of a metal hydride. The high-energy density, excellent power density, and long cycle life of Ni/MH batteries make them a leading technology as the battery power source [33]. The aim of the present research is to study the influence of the microstructure on the electrochemical behaviour of the as prepared alloys.

## EXPERIMENTAL

In order to produce TiFe alloys, powders of Fe (99.5%) and Ti (99.7%) in suitable stoichiometric amounts were mixed together in the vial of a high-energy Fritsch planetary equipment (Pulverisette 5). A mass ratio of 10:1 of ball to powder was used. The milling process was executed under a protective argon atmosphere and liquid n-heptane for process control agent. Five different milling times (10, 15, 20, 30 and 40 h) were applied so as to produce powders with different morphology and microstructure.

The mechanically alloyed powders obtained after milling of 10, 15, 20, 30 and 40 hours were microstructurally characterized by X-ray diffraction (XRD) using Philips-APD 15 powder diffractometer with Cu-K $\alpha$  radiation, scanning electron microscopy (SEM, JEOL-5510), differential thermal analysis (DTA – Perkin Elmer), differential scanning calorimetry (Perkin-Elmer DSC 7) and a three-channel software controlled galvanostatic setup (developed in IIES-BAS). The milled powders were used to prepare metal-hydride electrodes by mixing 100 mg alloy with 30 mg Teflonized carbon black (VULKAN 72 with 10 wt% PTFE). Then, 1000 kg cm<sup>-2</sup> of pressure was applied on the mixture placed on the nickel mesh. The electrode was charged and discharged galvanostatically in a three- electrode cell in 30 wt % water solution of KOH at room temperature. The reference electrode was Hg/HgO and the counter electrode was a high-surface nickel foam sheet. The charge and discharge current density was 100 mA g<sup>-1</sup> and 20 mA g<sup>-1</sup>, respectively.

## RESULTS AND DISCUSSION

Five TiFe alloys were obtained by mechanical alloying method (MA) with differing milling duration times (10, 15, 20, 30 and 40 h). The X-ray diffraction patterns of the milled alloys are presented in Fig. 1. Milling for 10 hours leads only

to reduction in the iron and titanium grain size. The average grain size, calculated by the Scherrer equation, for Fe and Ti is 35 nm and 55 nm, respectively. With increased milling time the diffraction peaks of Fe and Ti additionally broaden and partially overlap. That is an indication of a solid-state reaction resulting in the formation of TiFe. The powder milled for 15 hours contains about 25 wt% highly disordered TiFe phase. Milling for 20 hours leads to a substantial increase in the amount of TiFe (~80 wt%) which has a nanocrystalline microstructure with dimensions of 3–4 nm. During further milling of up to 30 hours we observe that the quantity of TiFe did not change noticeably, although the TiFe nanocrystals become slightly larger – with dimensions of 4–5 nm. When the milling time is increased up to 40 hours we observe an additional widening of the diffraction peaks and an increase of the size of TiFe nanocrystalline up to 5–6 nm. The diffraction peak of nanocrystalline Fe is present in all milling times, which probably means that Ti dissolves into TiFe. This is confirmed by the shift of the TiFe main diffraction peak ( $2\theta = 43$ ) to smaller angle (see Fig. 1). The average size of the powders was reduced from 50  $\mu\text{m}$  to <1  $\mu\text{m}$  after 30–40 hours of grinding. The end product of milling consists mainly of nanocrystalline fcc TiFe with CsCl-type structure. Presence of nanocrystalline Fe was also detected.

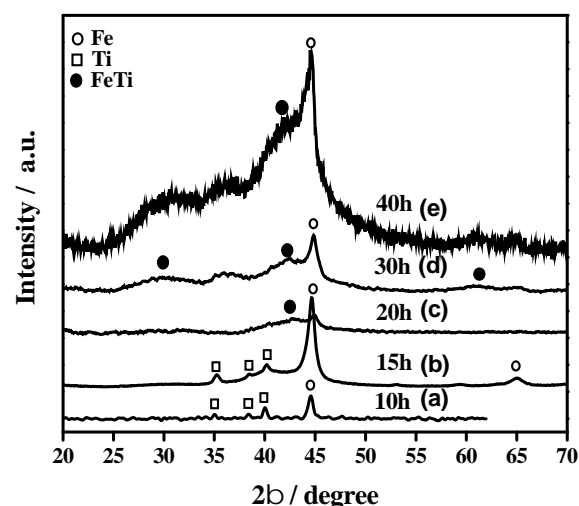


**Fig.1.** X-ray patterns of the TiFe powders milled for different times.

To study the thermal behaviour of the ball-milled alloys a DTA analysis of the as-milled (20 h and 30 h milled) alloys was carried out (Fig. 2). Several exothermic peaks in the range 350–550°C are clearly observed. That is probably a result from processes of crystallisation of amorphous (disordered) phase and/or with growth of existing nanocrystals formed during the mechano-chemical

treatment. The observed processes are in correspondence with the ones previously obtained by Zaluski et al. [34-35]. A high possibility is present that a solid-state reaction resulting in TiFe formation during the annealing of the ball milled material. In the present investigation the enthalpy state deviations related to the exothermic reactions, detected by DTA, are substantially larger for the alloy milled for 30 h in comparison to that milled for 20 h (see Fig. 2). That demonstrates significant differences in the amount of the amorphous (disordered) phase in both alloys. The exothermic effects obtained for the sample milled for 15 h are substantially smaller than those of the 20 and 30 h milled samples. Thus, they are much more difficult to detect via DTA, giving incentives that the amount of the amorphous phase in the samples milled for 10 h and 15 h is negligibly small. In order to analyse thoroughly the origin of the observed exothermic reactions, a XRD analysis of samples annealed after each of the thermal effects has to be carried out. A detailed study on the possibility for producing TiFe alloys with defined microstructures by combining the processes of ball milling with subsequent annealing is in underway.

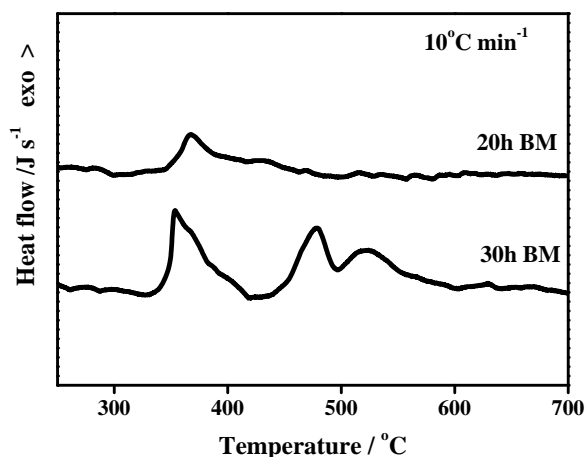


Fig. 2. DTA analysis of as-milled alloys.

For investigation of the hydrogen-sorption properties of the synthesised TiFe alloys from the gas phase a differential scanning calorimetry (High-pressure DSC) under hydrogen pressure was used. That method allows the registration of the processes of hydrogen absorption and desorption in the investigated materials, as well as the determining of the temperature intervals at which the reactions occur. A thermogram of the base TiFe alloy (30 h BM) is shown on Fig. 3 in which it is observed that at 25 atm of hydrogen pressure there is a clearly pronounced low-temperature absorption process in the temperature range of 120-220 and a second absorption process at around 300. The obtained high-temperature exothermic peak is related to the

formation of the hydride phase (TiH<sub>x</sub>) during interaction with the present in the alloy unbound titanium with hydrogen. For the period of several cycles (absorption / desorption) the exothermic effects resulting from the absorption of hydrogen from the alloy decrease due to partial oxidation of the alloys during the calorimetric analysis.

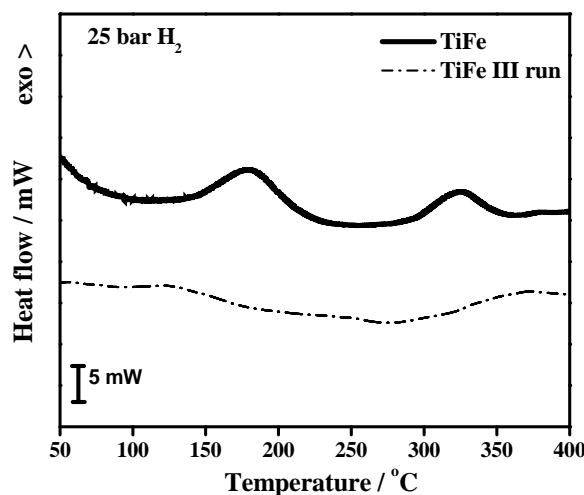


Fig. 3. DSC of 30h milled TiFe alloy.

In Fig. 4 a thermogram at 0.1 bar H<sub>2</sub> of the initially hydrated TiFe alloy is presented. A large and endothermic peak is observed in the temperature range of 150-350 caused by the desorption of the dissolved hydrogen in the fcc TiFe phase. The clearly expressed peak at around 280 corresponds to the decomposition of the formed during hydration hydride. As a result of the enthalpy from decomposition it may be concluded that the formed in these predefined conditions (25 atm H<sub>2</sub>) hydride is in minor quantities (fewer than 10 vol. %).

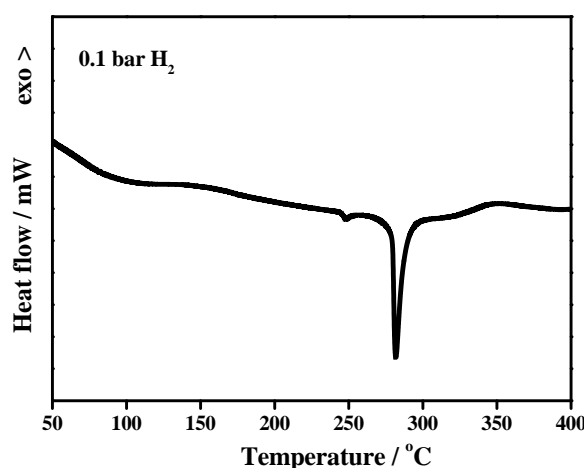
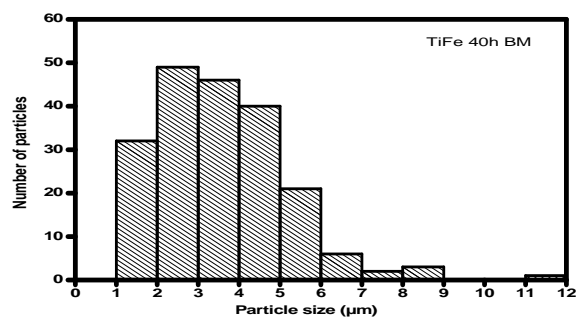
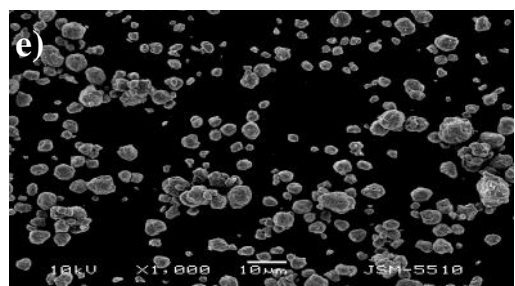
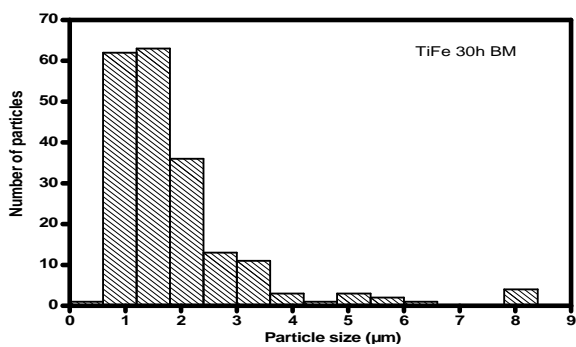
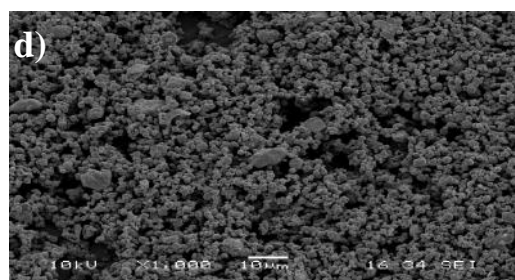
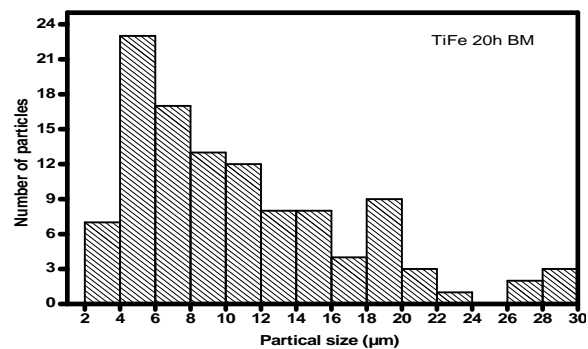
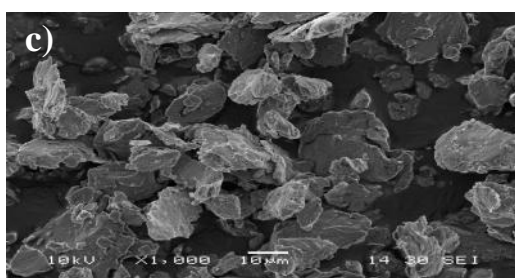
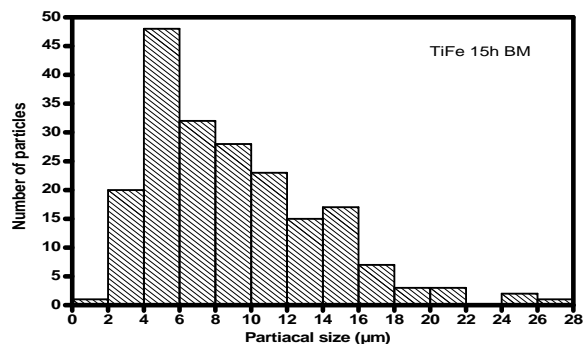
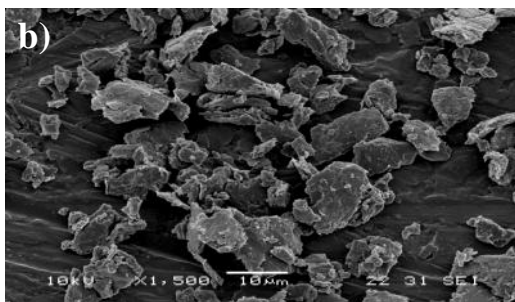
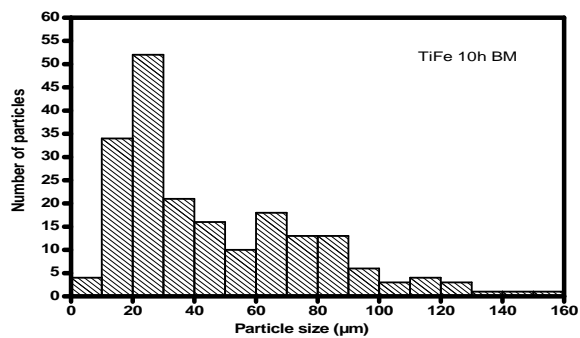
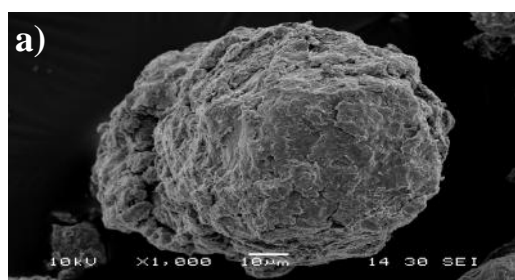


Fig. 4. Thermogram of TiFe alloy.

Scanning electron microscopy (SEM) analysis showed particles size in the range of 10–100 μm with an average particle size of about 50 μm for the sample milled for 10 hours and shown in Fig. 5a.



**Fig. 5.** SEM micrographs and particle size distribution of the TiFe powders milled for (a) 10 h (b) 15 h (c) 20 h, (d) 30 h and 40 h.

On the one hand, the particles are agglomerates of smaller particles with almost spherical (oval) shape. On the other hand the powders milled for 15 and 20 h contain particles with plate-like shape (shown in Fig. 5b,c). The rather dissimilar morphology of the powders milled for a different duration is due to a difference in the mechanical properties (and more specifically: hardness) of the materials, which is most clearly distinct between the samples milled for 10 hours and 15 hours. A spherical shape is also observed in the particles of powder milled for 30 hours, but the average size (1–2  $\mu\text{m}$ ) is significantly reduced in comparison to the particles milled for 10 hours only (Fig. 5d). After continuous milling of up to 40 hours an increase in the average particle size (2–3  $\mu\text{m}$ ) is observed which is possibly due to the agglomerate formation during the further ball milling (Fig. 5e).

During milling the particle size reduces progressively, as the first size reduction (between 10 and 15 h) is larger (Fig. 6).

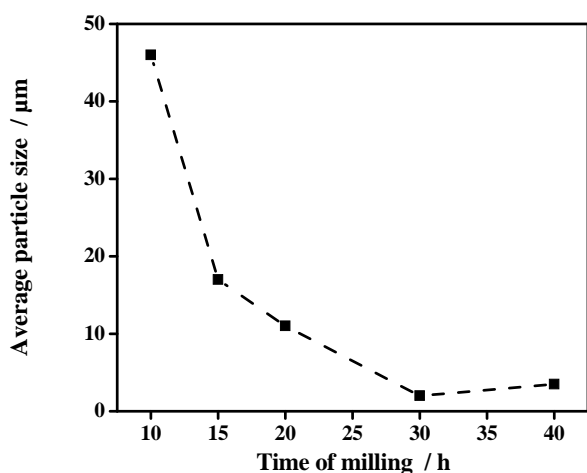


Fig. 6. Particle size vs. milling time.

The electrodes prepared from TiFe alloys with different microstructure were charged for 10 h at current density of  $100 \text{ mA g}^{-1}$  and discharged at  $20 \text{ mA g}^{-1}$  to cut-off potential of  $-400 \text{ mV}$  versus the reference electrode. Two discharge reactions were observed for all four alloys: the first at about  $-880 \text{ mV}$  and the second at about  $-700 \text{ mV}$ . While the first discharge reaction does not show a clear plateau, the second shows a near-horizontal line (Fig. 7). Clearly, the alloys contain two hydriding phases. Most probably these are the nanocrystalline and the amorphous phases, which may also differ slightly in their chemical composition. This result needs further investigation. The total discharge capacity as a function of charge/discharge cycle number is presented in Fig. 8. An initial discharge capacity increase with cycle number followed by a capacity decrease after a certain number of cycles is observed for all alloys. The discharge capacity

maxima appear at different cycle number for the different alloys.

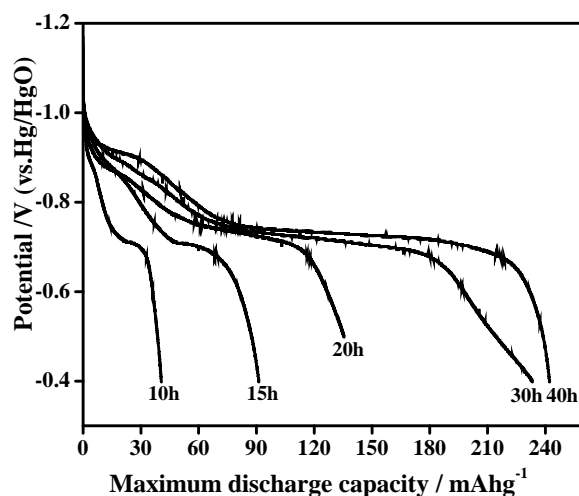


Fig. 7. Discharge curves of TiFe milled for different time 10, 15, 20, 25, 30 and 40 h.

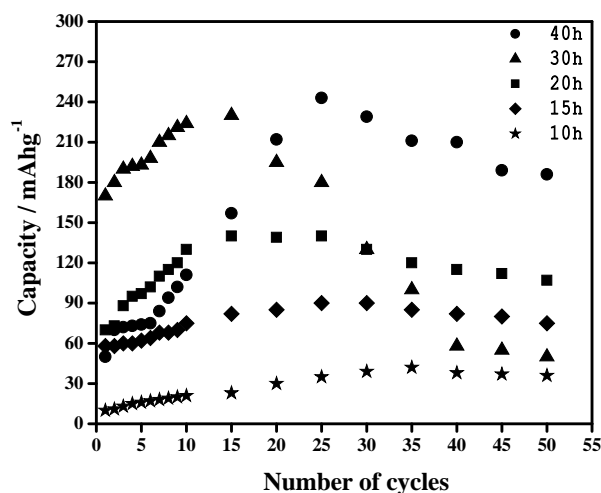


Fig. 8. Capacity as a function of cycle number for different as milled TiFe powders.

For the sample milled for 10 h the activation lasts about 35 charge/discharge cycles and the maximum capacity attained is  $40 \text{ mAh g}^{-1}$ . The alloy milled for 30 h has shorter activation period (15 cycles) and its maximum capacity is  $236 \text{ mAh g}^{-1}$ . The maximum discharge capacity of the alloy obtained at 40 h milling time does not differ substantially ( $240 \text{ mAh g}^{-1}$ ) from the one obtained for 30 h of milling. Nevertheless, it remains relatively stable for a long period of time. For 50 charge-discharge cycles the capacity decay is around 20%. That value is substantially higher than all capacity values published for this alloy composition [11]. As the milling duration increases, a decrease in the activation period is observed, as well as, an increase in the maximum discharge capacity. The large difference between the electrochemical capacity measured in the present work and in previous studies can only be due to the

microstructural difference. In this study we use composite nanocrystalline/amorphous TiFe alloys, which are acknowledged to be suitable for hydrogen storage. Moreover, the presence of nanocrystalline iron in the as-milled material might also be favourable for the hydriding process. The rate of capacity decrease, however, also increases with milling time (Fig. 8).

## CONCLUSIONS

Using the process of high-energy ball milling, nanostructured TiFe alloys with different morphology and microstructure were obtained. The evolution of the particle size was determined. The thermal stability and crystallisation of the as-milled nanocrystalline alloys were investigated and formation of an amorphous phase during milling was found. Strong dependence on the microstructure was observed in relation to the hydrogen capacity of the ball-milled nanostructured alloys. The alloy obtained from 40 hours of milling possesses the maximum discharge capacity which may be related to the increase of the average particle size in comparison to the alloy obtained from 10, 15, 20 and 30 hours of milling. This value of 240 mAh g<sup>-1</sup> is significantly higher than the ones obtained previously [11]. The investigated samples need activation, as the activation time shortens when refining the microstructure. The alloys milled for 20 and 30 hours demonstrate a noticeably poorer cycle life in comparison to those milled for 10 and 15 hours, which have similar stability during continuous charge/discharge cycling. That phenomenon is because of the presence of a larger amount of amorphous phase in the alloys milled for 20 and 30 hours. The material milled for 40 hours revealed discharge capacity comparable to that of alloy milled for 30 hours but its stability was greatly improved. That is most probably due to the formation of agglomerates at continuous milling between 30-40 hours.

## REFERENCES

1. K. Buschow, P. Bouten, A. Miedema, Hydrides formed from intermetallic compounds of two transition metals: a special class of ternary alloys, *Rep. Prog. Phys.*, **45**, 937 (1982).
2. T. Sakai, M. Matsuoka, C. Iwakura, Rare earth intermetallics for metal-hydrogen batteries. In: Gschneider Jr K A, Eyring L, editors. Handbook on the physics and chemistry of rare earth, vol. 21. Elsevier; 1995. p. 142.
3. H. Aoyagi, K. Aoki, T. Masumoto, Effect of ball milling on hydrogen absorption properties of FeTi, Mg<sub>2</sub>Ni and LaNi<sub>5</sub>, *J. Alloys Compd.*, **231**, 804 (1995).

4. M. Bououdina, D. Grant, G. Walker, Review on hydrogen absorbing materials d structure, microstructure, and thermodynamic properties, *Int. J. Hydrogen Energy*, **31**, 177 (2006).
5. H. Hotta, M. Abe, T. Kuji, H. Uchida, Synthesis of TiFe alloys by mechanical alloying, *J. Alloys Compd.*, **439**, 221 (2007).
6. D. Yan, G. Sandrock, S. Suda, Activation of Zr<sub>0.5</sub>Ti<sub>0.5</sub>V<sub>0.75</sub>Ni<sub>1.25</sub> alloy electrodes by hot alkaline solutions, *J. Alloys Compd.*, **216** (1994).
7. J. Kleparis, G. Wojcik, A. Czerwinski, J. Skowronski, M. Kopczyk, M. Beltowska-Brzezinska, Electrochemical behavior of metal hydrides, *J. Solid State Electrochem.*, **5**, 229 (2001).
8. S. Kulkova, D. Valujsky, J. Kim, L. Geunsiik, Y. Koo, Optical properties of TiNi, Ti Co and TiFe thin films, *Physica B*, **304**, 186 (2001).
9. R. Reilly, R. Wiswall, Formation and properties of iron titanium hydride, *Inorg Chem*, **13**, 218 (1974).
10. M. Abe, T. Kuji, Hydrogen absorption of TiFe alloy synthesized by ball milling and post-annealing, *J. Alloys Compd.*, **446-447**, 200 (2007).
11. M. Jurczyk, Nanostructured electrode materials for Ni-MH<sub>x</sub> batteries prepared by mechanical alloying, *J. Mater. Sci.*, **39**, 5271 (2004).
12. R. Wakabayashi R, Sasaki, T. Akiyama, Self-ignition combustion synthesis of oxygen-doped TiFe, *J. Alloys Compd.*, **34**, 5710 (2009).
13. J. Kim, S. Oh, G. Lee, Y. Koo, S. Kulkova, V. Egorushkin, Theoretical study of electronic structure and H adsorption properties in TiFe thin films with Pd coating, *Int. J. Hydrogen Energy*, **29**, 87 (2004).
14. G. Sandrock, P. Goodell, Surface poisoning of LaNi<sub>5</sub>, FeTi and (Fe, Mn) Ti by O<sub>2</sub>, Co and H<sub>2</sub>O, *J. Less-Common Met.*, **73**, 161 (1980).
15. N. Cui, P. He, J. Luo, Magnesium-based hydrogen storage materials modified by mechanical alloying, *Acta Mater.*, **47**, 3737 (1999).
16. T. Bai, S. Han, X. Zh, Y. Zhang, Y. Li, A. Zhang, Effect of duplex surface treatment on electrochemical properties of AB<sub>3</sub>-type La<sub>0.88</sub>Mg<sub>0.12</sub>Ni<sub>2.95</sub>Mn<sub>0.10</sub>Co<sub>0.55</sub>Al<sub>0.10</sub> hydrogen storage alloy, *W. Mater. Chem. Phys.*, **117**, 173 (2009).
17. Y. Li, S. Han, J. Li, X. Zhu, L. Hu, The effect of Nd content on the electrochemical properties of low-Co La-Mg-Ni-based hydrogen storage alloys, *J. Alloys Compd.*, **458**, 357 (2008).
18. J. Ma, H. Pan, Y. Zhu, S. Li, C. Chen, Q. Wang, Electrochemical properties of La<sub>0.9</sub>Sm<sub>0.1</sub>Ni<sub>(5.0-x)</sub>Co<sub>x</sub> (x=2.0, 2.5, 3.0) hydride electrode alloys, *Electrochem. Acta*, **46**, 2427 (2001).
19. H. Ye, Y. Huang, T. Huang, H. Zhang, Influence of the boron additive on the electrochemical properties of the MnNi<sub>3.55</sub>Co<sub>0.75</sub>Mn<sub>0.4</sub>Al<sub>0.3</sub> hydrogen storage alloy, *J. Alloys Compd.*, **330**, 866 (2002).
20. M. Wang, Y. Zhang, L. Zhang, L. Sun, Z. Tan, F. Xu, H. Yuan, T. Zhang, *J. Power Sources*, **159**, 159 (2006).
21. C. Khaldi, H. Mathlouthi, J. Lamloumi, J. Percheron-Guegan, J. Electrochemical study of cobalt-free AB<sub>5</sub>-

- type hydrogen storage alloys, *Int. J. Hydrogen Energy*, **29**, 307 (2004).
22. B. Ratnakumar, C. Withan, R. Bowman, A. Hightower, B. Fultz, Electrochemical Studies on  $\text{LaNi}_{5-x}\text{Sn}_x$  Metal Hydride Alloys, *J. Electrochem. Soc.*, **143**, 2578 (1996).
  23. G. Zheng, B. Popov, R. White, Determination of Transport and Electrochemical Kinetic Parameters of Bare and Copper-Coated  $\text{LaNi}_{4.27}\text{Sn}_{0.24}$  Electrodes in Alkaline Solution, *J. Electrochem. Soc.*, **143** (3), 834 (1996).
  24. M. Ciureanu, D. Moroz, R. Ducharme et al. Electrochemical Studies of Amorphous  $\text{Ni}_{64}\text{Zr}_{36}$  Hydride Electrodes, *Z. Phys. Chem. Bd*, **183**, 365 (1994).
  25. J. Strom-Olsen, Y. Zhao, D. Ryan, Hydrogen diffusion in amorphous  $\text{NiZr}$ , *J. Less-Common Met.*, **172**, 922 (1991).
  26. M. Tliha, H. Mathlouthi, C. Khalid, J. Lamloumi, A. Percheron, Electrochemical properties of the  $\text{LaNi}_{3.55}\text{Mn}_{0.4}\text{Al}_{0.3}\text{Co}_{0.4}\text{Fe}_{0.35}$  hydrogen storage alloy, *J. Power Sources*, **160**, 1391 (2006).
  27. M. Jurczyk, W. Rajewski, W. Majchrzycki, G. Wojcik, Mechanically alloyed  $\text{MmNi}_5$ -type materials for metal hydride electrodes, *J. Alloys Compd.*, **290**, 262 (1999).
  28. J. Willems, K. Buschow, From permanent magnets to rechargeable hydride electrodes, *J. Less-Common Met.*, **129**, 13 (1987).
  29. T. Sakai, H. Miyamura, N. Kuriyama, A. Kato, K. Oguro, H. Ishikawa, Metal Hydride Anodes for Nickel-Hydrogen Secondary Battery, *J. Electrochem. Soc.*, **137**, 795 (1990).
  30. H. Pan, J. Ma, C. Wang, C. Chen, Q. Wang, Effect of Co content on the kinetic properties of the  $\text{MmNi}_{4.3-x}\text{Co}_x\text{Al}_{0.7}$  hydride electrodes, *Electrochim. Acta*, **44**, 3977 (1999).
  31. M. Latroche, Y. Chabre, A. Percheron, O. Isnard, B. Knop, Influence of stoichiometry and composition on the structural and electrochemical properties of  $\text{AB}_{5+y}$ -based alloys used as negative electrode materials in Ni-MH batteries, *J. Alloys Compd.*, **330**, 787 (2002).
  32. A. Anani, A. Visintin, S. Srinivasan, A. Appleby, H. Lim, Microcalorimetry Study of Ni/ $\text{H}_2$  Battery Self-Discharge Mechanism, *J. Electrochem. Soc.*, **139**, 985 (1992).
  33. M. Tliha, C. Khalidi, S. Boussami, N. Fenineche, O. Kedim, H. Mathlouthi, J. Lamloumi, Kinetic and thermodynamic studies of hydrogen storage alloys as negative electrode materials for Ni/MH batteries: a review, *J. Solid State Electrochem.*, **18**, 577 (2014).
  34. L. Zaluski, P. Tessier, D. Ryan, C. Doner, A. Zaluska, J. Strom-Olsen, M. Trudeau, R. Schulz R, *J. Mater. Res.*, **8**, 3059 (1993).
  35. P. Tessier, L. Zaluski, A. Zaluska, J. Strom-Olsen, R. Schulz, *Mater. Sci. Forum*, **225-227**, 869 (1996).

TiFe

1\* , 2 , 1 , 1 , 1

1 “ ” 10, 1113, “ ,

2 “ ” 1164, I,

6 2017 ; 3 2017 .

( )

- TiFe

30-40 50 - 1 Fe.

/

40

30 ,